Composites Part C: Open Access 14 (2024) 100467

Contents lists available at ScienceDirect

Composites Part C: Open Access

journal homepage: www.sciencedirect.com/journal/composites-part-c-open-access

A new method for rapidly capturing the strength and full nonlinear response of partially interacting steel–concrete composite beams

Marco Lamberti [a,b,*], Ghani Razaqpur [c,d]

[a] ENEA, Research Centre Brasimone, Italy
[b] Aix-Marseille University, CNRS, Centrale Marseille, LMA, Marseille, France
[c] Professor Emeritus, Department of Civil Engineering, McMaster University, Hamilton, ON, Canada
[d] Former Chair Professor, College of Environmental Science and Engineering, Nankai University, Tianjin, China

ARTICLE INFO

Keywords:
Analysis
Concrete
Composite
Non-linear
Partial interaction
Steel

ABSTRACT

A semi-analytical procedure is presented for predicting the complete flexural response of partially interacting steel–concrete composite beams up to failure. The governing equation of the Euler–Bernoulli beam theory is solved wherein concrete, steel and the shear connectors joining the concrete slab to the steel beam are assumed to have nonlinear stress-deformation relationships. The adopted constitutive relationship for the connectors allows for partial or full composite action. The solution is applicable to beams and one-way slabs subjected to concentrated or uniform load and/or their combination. The governing equation is numerically solved by satisfying the equilibrium and compatibility requirements along the member. For the reinforced concrete part of the composite beam, a nonlinear moment–curvature relationship is developed that accounts for concrete nonlinearity in compression and for cracking and tension-stiffening in tension as well as for steel reinforcement nonlinearity. The steel profile is assumed to have a bilinear elasto–plastic strain-hardening moment–curvature relationship. Comparison of the proposed model results with the corresponding experimental load–deflection curves and interfacial shear–slip curves of several beams tested by others shows good agreement. The relative simplicity, efficiency and easy application of the present solution make it possible to accurately predict the failure load, interfacial slip and full nonlinear response of partially interacting composite beams.

1. Introduction

Steel–concrete composite members are considered an attractive option for the construction of buildings and bridges as they take advantage of the high tensile strength and shear capacity of steel and the high compressive strength of concrete as well as avoiding the early buckling of the compression flange of the steel section. Furthermore, cost-effectiveness and ease of construction due to minimal formwork and non-necessity of shoring make them very popular. Consequently, a large portion of the short and medium span bridges built around the world involve this form of construction. However, such construction may be structurally less attractive for members that experience large and/or frequent moment reversal, causing significant tension in the concrete slab [1].

In steel–concrete composite flexural members, the steel girder is typically connected to the reinforced concrete slab using steel shear connectors to ensure a high degree of composite action and to allow the horizontal shear forces to be transferred between the girder and the slab. Typically, the connectors consist of headed shear studs that are welded to the top flange of the steel girder and embedded in the concrete slab [2]. The size, stiffness, strength and spacing of the studs will affect the degree of composite action, and the strength and stiffness of the composite member. Experiments have shown [3] that the interfacial slip between the concrete slab and the steel girder can occur even at low load levels due to the finite rigidity of the connectors. This phenomenon results in the so-called "partial interaction" or partial composite action.

Several models are available in the literature for computing the ultimate strength and deformations of composite members experiencing partial interaction [4–9]. The earliest of these was presented by Newmark et al. [4] where the steel girder and the concrete slab were considered as two conventional beams, connected by means of linear springs capable of transferring the horizontal shear at the beams interface. The differential equation governing the flexural behavior of the joined beams was formulated. Several methods can be employed to solve

* Corresponding author.
E-mail address: marco.lamberti@enea.it (M. Lamberti).

https://doi.org/10.1016/j.jcomc.2024.100467

Available online 3 May 2024
2666-6820/© 2024 The Author(s). Published by Elsevier B.V. This is an open access article under the CC BY-NC-ND license (http://creativecommons.org/licenses/by-nc-nd/4.0/).

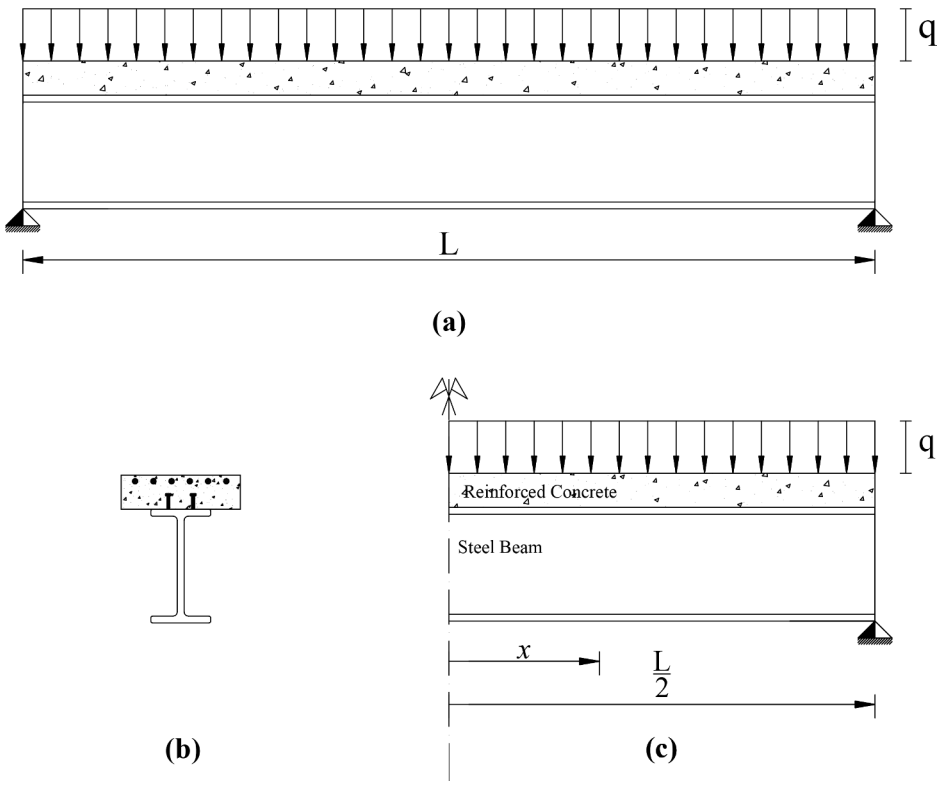

Fig. 1. Typical steel–concrete composite beam: (a) frontal view; (b) section; (c) reference system.

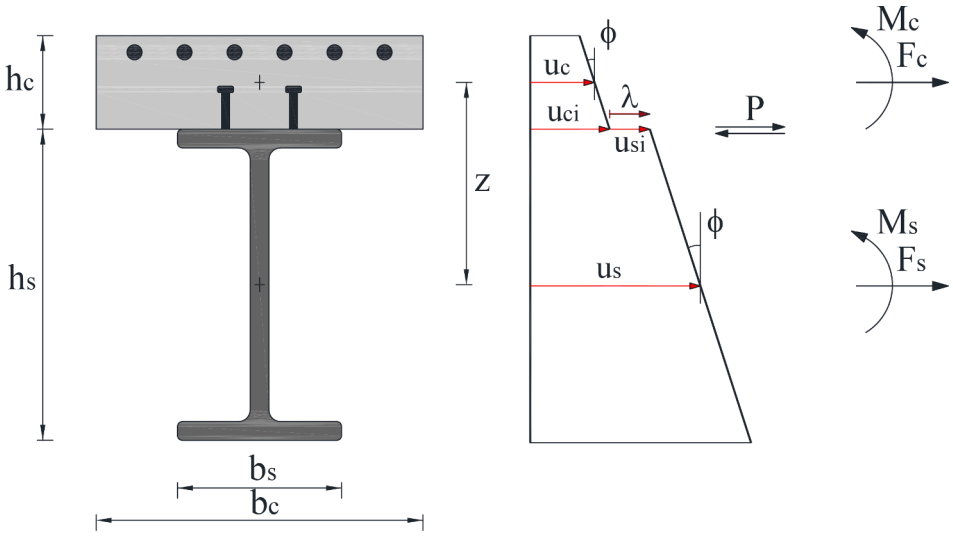

Fig. 2. Transverse section of steel–concrete composite beam.

the equation and to perform the analysis for various girder-slab assemblies. Subsequently, others primarily applied the finite element method to analyze composite bridges, but most of these have used commercially available software and linear elastic analysis, assuming full composite action (Eom and Nowak [5], Phuvoran et al. [5], Yousif and Hindi [7]). Other researchers developed analytical methods for modeling composite beams and frames as summarized by Spacone and El-Tawil [8], assuming a linear or bilinear shear–slip relationship for the concrete-steel interface (Foraboschi [9]).

Additionally, analytical models have been developed, based on the conventional Euler–Bernoulli beam theory, coupled with interlayer slip [10–13]. Wu et al. [10] used the classic linear-elastic partial-interaction theory for composite steel and concrete members to evaluate the response of composite beams and columns under flexure. Girhammar et al. [11,12] applied the same beam theory to evaluate the deflection of partially composite beams and beam-columns wherein both the steel and concrete were assumed to behave linear elastically. Jian-Ping et al. [13] derived the stiffness matrix of composite beams considering the interlayer slips based on the kinematic assumptions of Timoshenko's beam theory. They developed a finite element model by assembling the local stiffness matrices and corresponding equivalent nodal forces. Once again, all the constituent materials were assumed to behave linear elastically. To account for the effects of shear deformations, Xu et al. [14,15] used Timoshenko's beam theory coupled with interlayer slip to

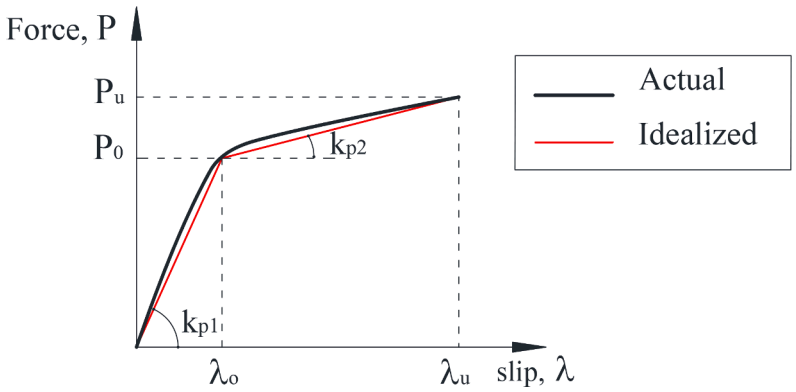

Fig. 3. Interfacial shear slip law used in the current study.

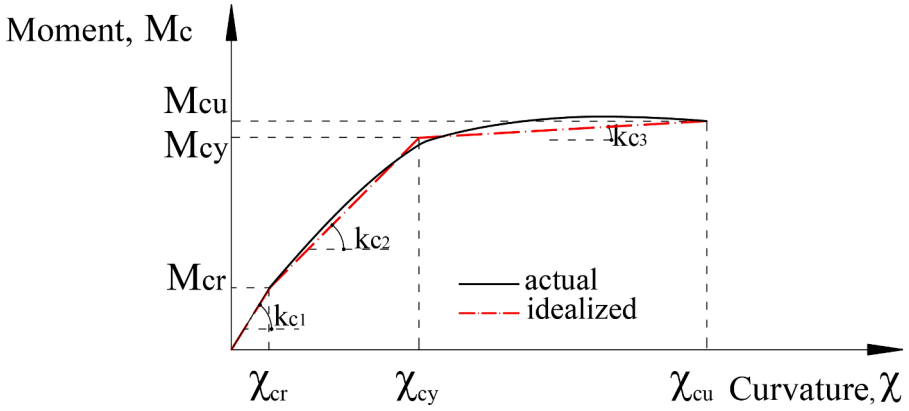

Fig. 4. Trilinear moment–curvature curve for an retrofitted RC section.

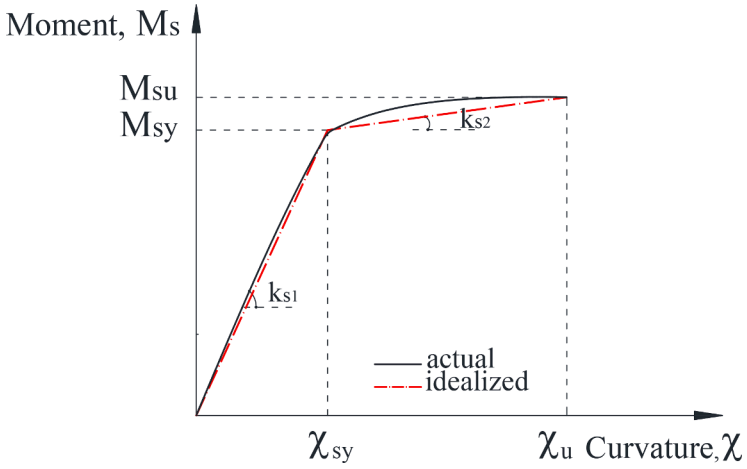

Fig. 5. Bilinear moment–curvature curve for steel section.

investigate the static, dynamic, and buckling behavior of partially interacting composite beams. Subsequently, Xu and Wang [16] formulated the minimum potential and complementary energy equations for the partial interaction of composite beams, as well as the variational principles for the free vibration and buckling of such members under the assumptions of linear elasticity. Schnabl et al. [17] also gave the analytical solutions for analyzing the elastic flexural response of a two-layer beam including shear deformation. Furthermore, Xu and Wang [18] compared the solutions of the governing equations of partial-interaction in composite flexural members based on the assumptions of Euler–Bernoulli and Timoshenko's beam theories and linear elasticity.

Numerical methods based on the stiffness method have been also developed to investigate partial interaction in composite beams [19–22]. Ayoub and Filippou [23] derived an inelastic beam element for the analysis of steel–concrete girders with partial interaction, subjected to monotonic or cyclic loads. The partial interaction was accounted for by an interface model with distributed force transfer characteristics. Faella et al. [24] developed the stiffness matrix of a composite beam element based on the exact solution of the governing equation formulated by Newmark, coupled with the assumption of linear shear–slip relationship for the connectors. Čas et al. [25] presented a formulation

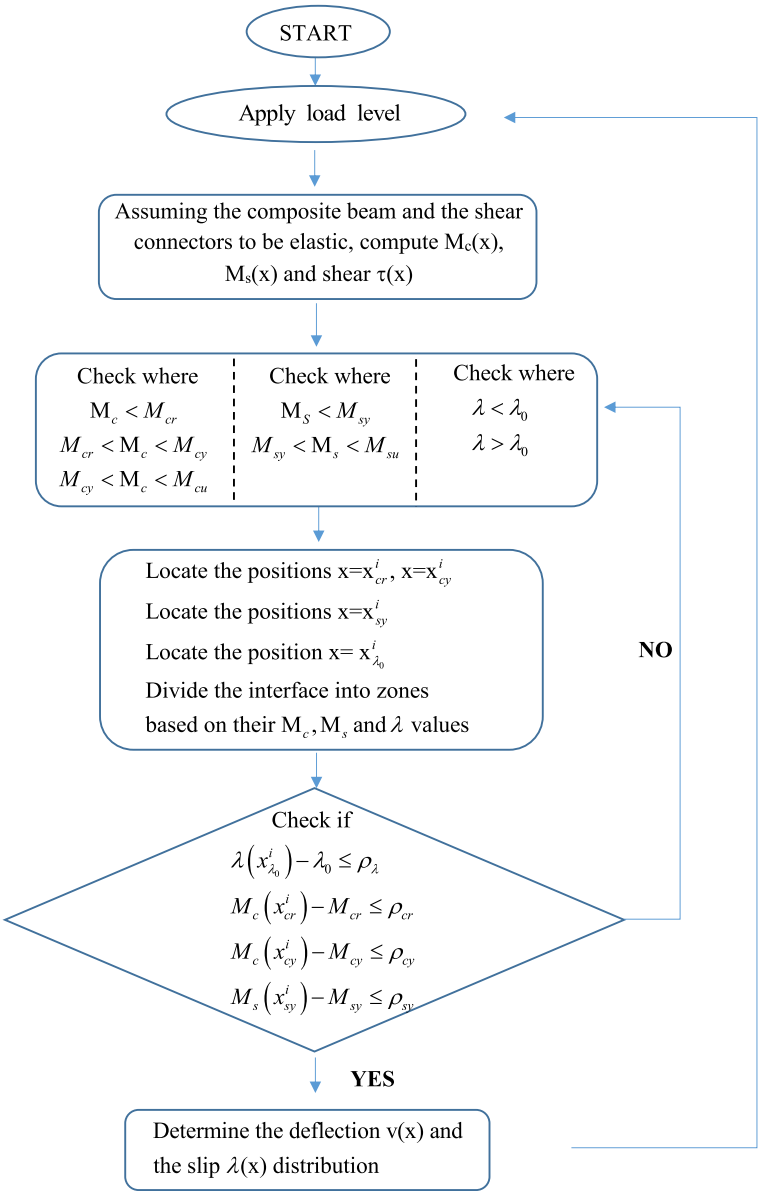

Fig. 6. Flow chart for the nonlinear computational procedure applied.

by employing a modified form of the principle of virtual work for the non-linear analysis of two-layer composite planar members admitting interlayer slip. Ranzi et al. [26] proposed an alternative formulation that essentially utilized the same concepts as contained in Newmark et al.'s seminal work [4]. Ranzi and Bradford [27] presented a formulation for the analysis of composite beam-columns based on the direct stiffness method, which considered partial interaction, assuming all the constituent materials, including the shear connectors, to be linear elastic. Subsequently, Ranzi and Zona [28] presented an analytical model for the analysis of steel–concrete composite beams by coupling the conventional beam theory for the reinforced concrete slab to the Timoshenko's theory for the steel girder that included the shear deformability of the latter. In the last work, the formulation accounted for creep and shrinkage effects in the concrete slab, but both the reinforcing steel and the steel girder were assumed to behave linear elastically. Jiang et al. [29] developed a two-node linear composite beam element for the steel–concrete composite beam with discrete shear connection. The element stiffness matrix was derived by applying the principle of total potential energy based on Timoshenko's beam theory and linear Lagrangian interpolation functions. Although both the concrete slab and the steel girder were assumed to obey Timoshenko's beam theory, the concrete slab was assumed to be linear elastic, lacking tensile strength, and the presence of steel reinforcement in the slab was neglected. Similarly, Nguyen et al. [30] derived the exact stiffness matrix for a two-layer Timoshenko's beam element with partial interaction. The shear connection was modeled through a linear relationship between the interface shear flow and the concomitant slip. Martinelli et al. [31] presented a closed-form formulation of the stiffness matrix and the equivalent nodal forces of an element, assuming linear elastic shear connectors, to analyze shear-flexible steel–concrete composite beams experiencing partial interaction.

Razaqpur et al. [32,33], developed a nonlinear finite element formulations for the analysis of composite steel–concrete bridges. In this formulation a special one-dimensional finite element with a nonlinear shear–slip relationship was developed to model shear connectors while the concrete slab and steel girder were discretized using layered facet shell elements. Both concrete and steel, including the reinforcing bars in the concrete slab, were assumed to behave nonlinearly, having defined failure criteria under a combined stress state. The applicability of the formulation was demonstrated in [34]. Other studies have been

Table 1
Geometrical and material properties of steel–concrete beam analyzed.

Property	Unit	Beam		
		Case (a) [48]	Case (b) [49]	Case (c) [50]
Steel section height, h_s	mm	250(i) 350	150	305
Steel section web thickness, t_w	mm	9 12	10	10
Steel flange width, b_s	mm	250(i) 350	130	152
Steel flange thickness, t_w	mm	14 19	10	10
Concrete slab width, b_c	mm	600	600	1220
Concrete slab thickness, h_c	mm	130 160	100	152
Reinforcement cover	mm	*30*	*30*	*30*
Tension steel area, A_s	mm^2	302	226	151
Compression steel area,A'_s	mm^2	302	226	151
Beam span length, L	mm	3700	4000	5490
Shear span, a	mm	1500	1600	–
Concrete strength, f'_c	MPa	38.97	34.4(ii) 35.2 74.9	42.5
Concrete ultimate strain, ε_{cu}	–	*0.035*(iii)	*0.035*	*0.035*
Concrete elastic modulus, E_c	GPa	37	*34*(ii) *34* *42*	35
Concrete cracking strain, ε_t	–	0.00015	0.00015	0.00014
Concrete tensile strength, f_t	MPa	4.01	*3.50* *3.50* *5.70*	3.55
Concrete curve-fitting factor, n	–	*2*	*2*	*2*
Concrete curve-fitting factor, k	–	*1*	*1*	*1*
Steel elastic modulus, E_s	GPa	*202*	200	200
Steel yield stress, f_y	MPa	358	338	250
Steel yield strain, ε_y	–	*0.0024*	*0.0024*	*0.0024*
Steel strain corresponding to its ultimate strength, ε_{su}	–	*0.075*	*0.075*	0.25
Steel profile yield strength, f_{sy}	MPa	267	341(ii) 450 450	260
Steel profile ultimate strength, f_{su}	MPa	402	390(ii) 481 481	410
Shear connector diameter, d_c	mm	16 19	16	*30*
Shear connector spacing, s	mm	140	230(ii) 200 200	110

Notes: (i) Duplicate beams designated as FBST-1 and FBST-2 had the smaller steel section while duplicate beams designated as FBST-4 and FBST-5 had the larger one.
(ii) These values correspond to beams designated as SCB1, SCB2 and SCB3, respectively.
(iii) Values in italics are assumed in the current analyses due to lack of reported values in the tests.

conducted by some researchers to analyze composite beams with partial interaction using either beam element formulation or the general finite element method similar to the above-described formulations [35–42]. In the latter studies, the constituent materials and the shear connectors were either treated as linear elastic or nonlinear elasto–plastic materials.

Although a great amount of research has been performed to analyze the flexural behavior of composite beams with partial interaction, the related analytical work can be classified into basically four categories: (i) formulations based on Newmark's equation which is based on the Euler–Bernoulli beam theory, linear elasticity and a linear shear–slip model, (ii) formulations based on the same assumptions as (i), but allowing for nonlinearity of concrete and steel, (iii) formulations based on Timoshinko's beam theory and linear elasticity, and (iv) formulations based on the general finite element method, using plate/shell elements alone or in combination with beam elements and an interfacial constitute law for the concrete slab-steel girder interface or discrete linear/nonlinear connector elements. The fourth type of modeling allows for capturing the full response of composite beams and structures, such as multi-girder bridges, but the beam type formulations are limited to isolated composite beams/columns or their assemblages joined at their ends. One of the difficulties with beam formulations is the exclusion of the effects of material nonlinearity in general and that of steel reinforcement in particular. Analyses that ignore nonlinearity will not be able to provide the full response of the member, including its ultimate strength. Ignoring the reinforcement of the concrete slab, will limit the use of beam type models to members under positive (sagging) bending moment only because the steel reinforcement generally dominates the bending resistance of composite beams under negative (hogging) moments. Although layered beam elements have been developed to address these issues, these elements require discretization of the steel girder and concrete slab into several layers or fibers and require the recalculation of the axial and flexural rigidity of the steel profile and concrete slab after each load increment and iteration, which can be time-consuming.

With respect to nonlinear analysis, it is necessary to assess the changes in the stiffness of a member under increasing load and to determine its ultimate strength accurately. The reduction in stiffness captured by nonlinear analysis will result in increased deflection, which can affect the member serviceability. Also, nonlinear analysis allows one to assess the redistribution of stresses between the constituent parts of a member, i.e. between the concrete slab and the steel girder in the case of steel–concrete composite beams. Stress redistribution will have implications with respect to the fatigue strength of the member. Albeit not covered by the proposed method, in the case of statically indeterminate structures, such as multi-girder continuous composite bridges or rigidly connected members in a frame, nonlinear analysis is necessary to correctly evaluate the redistribution of moments among the members. This knowledge is necessary for more accurately obtaining the ultimate strength and safety of the structure.

Non-linear constitutive models have to be formulated for a correct prediction of the actual behavior of actual structures allowing a correct and faithful prediction of experimental behavior [43–46].

Although commercial finite element (FE) software can be used to perform nonlinear analysis of structural components and assemblages, it is generally a time-consuming process, and the results need careful examination and interpretation. The authors believe that the proposed method is simpler and more expedient in the case of composite beams.

In the proposed formulation, the conventional beam theory that allows for partial interaction between the slab and the girder is adopted. Concrete is treated as a nonlinear material while steel, in the girder and as reinforcement in concrete, is considered to be an elasto–plastic strain hardening material. The slab-girder interface is represented by a bilinear elasto–plastic shear–slip law. To simplify the solution and make the method more appealing in practical applications, the actual nonlinear moment–curvature relationship for concrete slab is idealized by a trilinear curve to represent the uncracked, crack-unyielded and cracked-yielded states of the reinforced concrete section. To capture the beam full response, an incremental-iterative approach is adopted. The latter approach allows for capturing the full response of a composite beam rapidly and accurately. It will be shown that notwithstanding the adopted simplifications, the predictions of the model agree remarkably well with available experimental data for beams tested in bending by others.

2. Analytical formulation

Fig. 1 shows a typical steel–concrete composite beam, characterized by a span L and subjected to a uniformly distributed load q. The steel girder is assumed to be connected to the concrete slab by means of shear connectors along their interface, as depicted in Fig. 1(b). Due to symmetry, only half of the beam length is considered, Fig. 1(c), in the development of the current formulation. However, the proposed

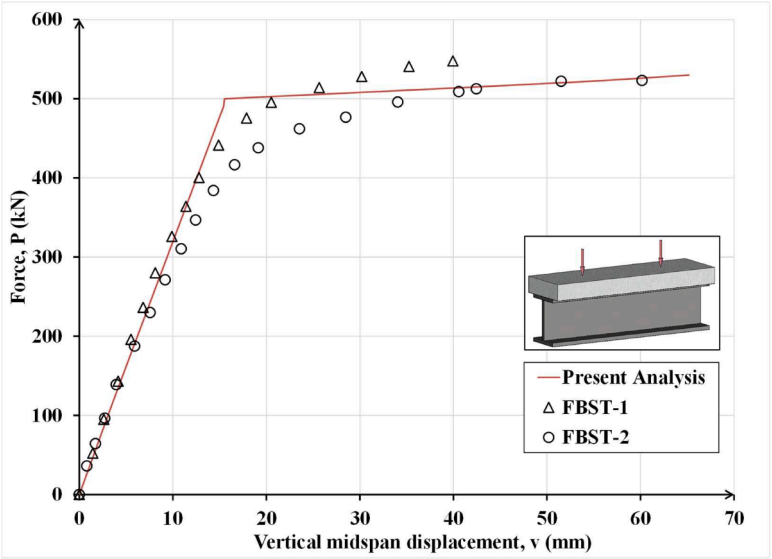

Fig. 7. Comparison of computed and experimental load–deflection curves for beam FBST-1 and FBST-2 in case (a).

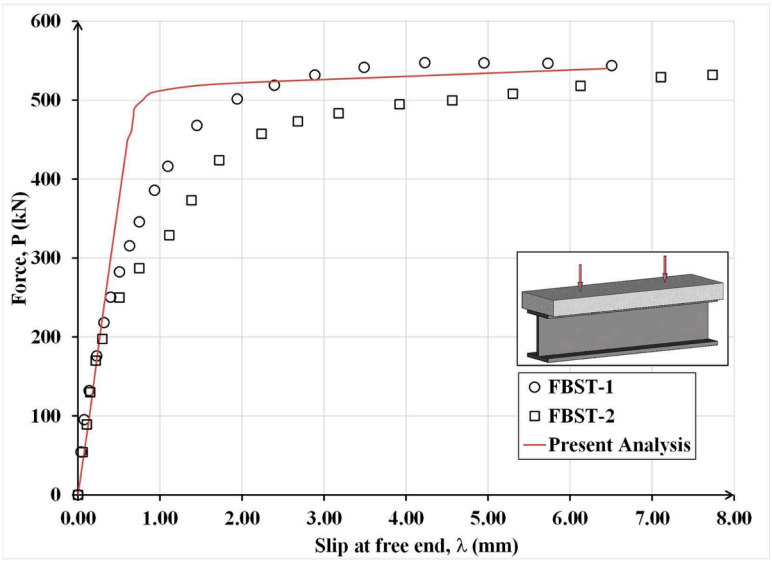

Fig. 8. Computed and experimental load–slip curve for duplicate beam FBST-1 and FBST-2 in case (a).

formulation is not theoretically restricted to symmetrical or uniformly loaded beams, but these restrictions are imposed to make the presentation clear and simple.

A typical cross-section of a steel–-concrete composite beam, subjected to an external moment, is depicted in Fig. 2. Observe that F_c, and M_c are the force and moment resultants of the stresses in the concrete and steel reinforcement, acting through the centroid of the concrete section, while F_s, and M_s are the force and moment resultants of the stresses in the steel profile, acting through its centroid.

The above moments represent the contribution of the slab and the steel profile, acting as non-composite elements, to the resisting moment of the composite section. The moment produced by the couple F_c and F_s is the additional resistance due to composite action. Moments M_c and M_s can be obtained from the moment–curvature relationship of the isolated concrete and steel section, respectively. The force P represents the resultant of the longitudinal shear stresses resisted by the shear connectors. Since there is no external axial load acting on the section, for longitudinal equilibrium at any section, the resultant force F_c in the concrete must be equal and opposite to the resultant force F_s in the steel. Furthermore, each of these forces are equal to P, which means that F_c and P constitute a couple acting on the slab and F_s and P forming another couple acting on the steel profile. This means that both the slab and the steel profile are subjected to pure moment and no axial load is acting on them.

Let the centroidal axial displacement of the concrete section and the steel profile be u_c and u_s, respectively. Then, the slip λ at the steel–-concrete interface can be expressed as

$$\lambda = u_{si} - u_{ci} = u_s - u_c - \phi z \tag{1}$$

where u_{ci} and u_{si}, respectively, represent the axial displacement of the concrete and steel at their interface, ϕ is the section rotation and z is the distance between the centroids of the concrete section and the steel profile. It is important to point out that in the present model, in compliance with the conventional beam theory, the concrete section and the steel profile are assumed to have equal vertical displacement and rotation at any section.

Considering the moment equilibrium of the composite cross section, the external moment M_e is equilibrated at any section by the sum of the

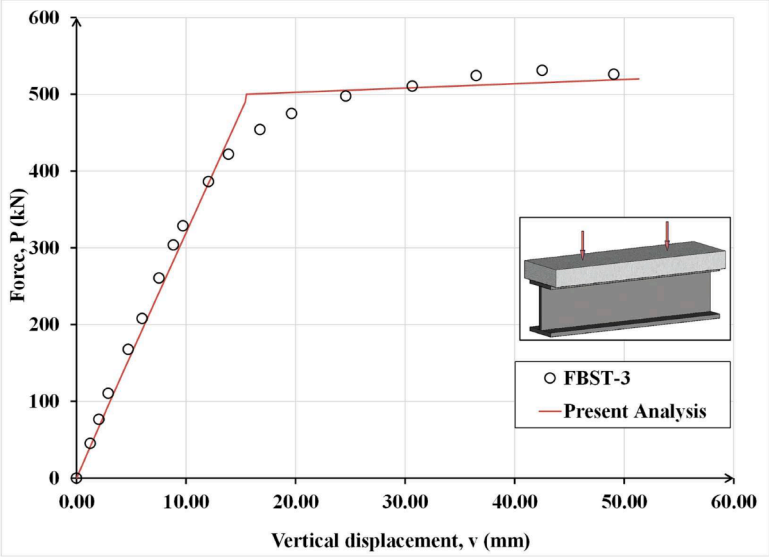

Fig. 9. Computed and experimental load–slip curve for beam FBST-3 in case (a).

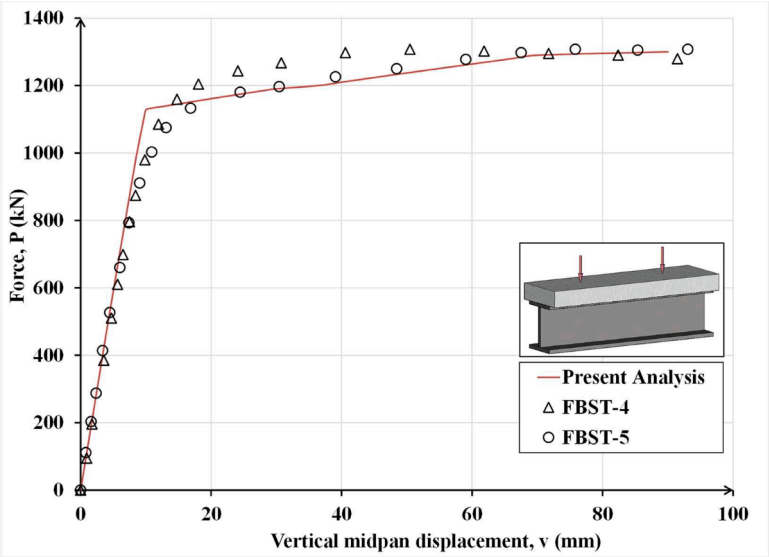

Fig. 10. Comparison of computed and experimental load–deflection curve for beam FBST-4 and FBST-5 in case (a).

resisting moments of the concrete section and the steel profile acting as non-composite sections, plus the additional moments generated by the eccentricity of the axial forces F_c and F_s as expressed by Eq. (2):

$$M_e = M_c + M_s + F_s d_s - F_c d_c = M_c + M_s + Pz \tag{2}$$

where the compressive force and the tensile force can be expressed as:

$$F_c = C_{cc} + C_{cs} - T_{cc} - T_{cs} \tag{3a}$$

$$F_s = T_{ss} - C_{ss} \tag{3b}$$

From the equilibrium of the internal axial forces

$$F_s = -F_c = P \tag{4}$$

The moment arms d_s and d_c in Eq. (2) represent the distance between the interface and the centroid of the concrete and steel, respectively. In the above equations, C_{cc} and C_{cs} are the resultant compressive forces resisted by the concrete and the steel reinforcement, respectively, while T_{cc}, and T_{cs} are the resultant tensile forces resisted by the concrete and the steel reinforcement, respectively. Forces T_{ss} and C_{ss}, are the resultant tensile and compresses forces, respectively, resisted by the steel profile.

From equilibrium of the horizontal forces acting on the steel profile, Fig. 2, the interfacial shear flow is given by

$$\frac{dF_s}{dx} = \frac{P}{s} = \tau \tag{5}$$

where τ is the interfacial shear flow and s is the connectors spacing. Notice, in the current formulation the origin of the coordinate x is located at midspan. The interfacial shear is a function not only of the slip λ at the steel–concrete interface but also of the shear connector mechanical and geometric properties. To model the constitutive behavior of the shear connectors, the following nonlinear shear force-slip relationship, proposed by Ollgard et al. [47], is adopted

$$P = P_u\left(1 - e^{-0.709\lambda}\right)^{0.4} \tag{6a}$$

$$P_u = \frac{1}{2}A_{sc}\sqrt{f_c E_c} \tag{6b}$$

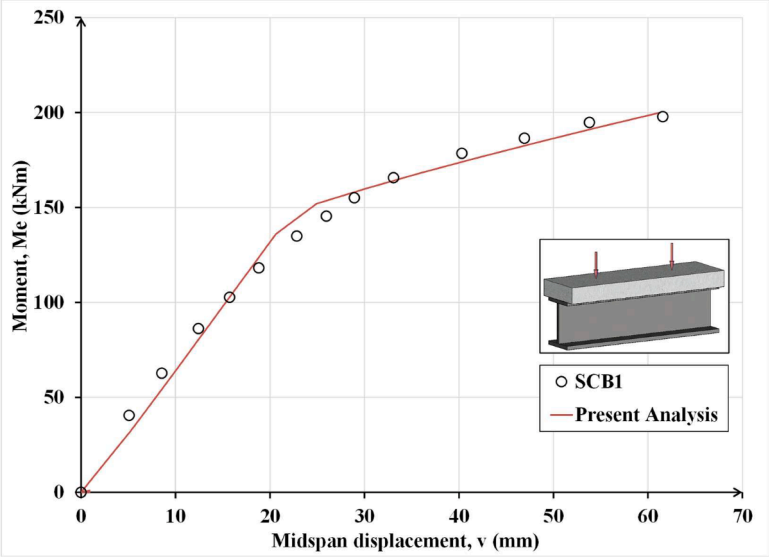

Fig. 11. Computed and experimental mid-span moment–displacement curve for beam SCB1 in case (b).

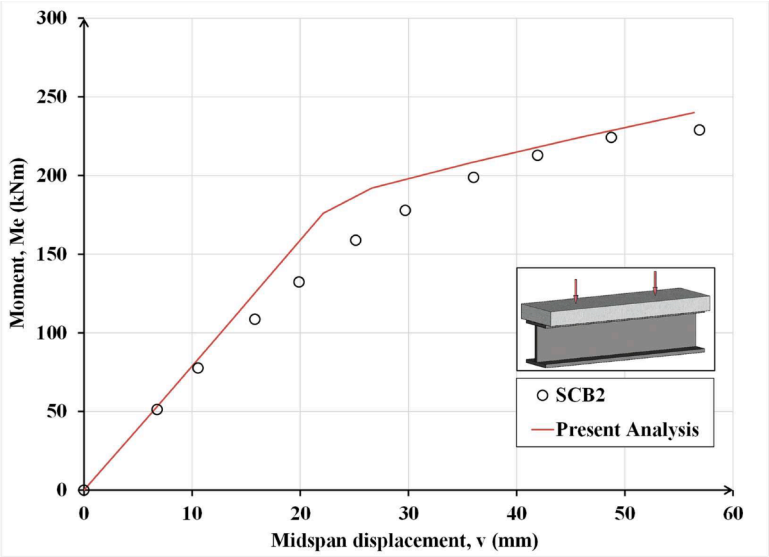

Fig. 12. Computed and experimental midspan moment–displacement curve for beam SCB2 in case (b).

where P_u is the maximum or ultimate shear resistance of the connector, A_{sc} is its area, f_c the concrete compressive strength and E_c is its elastic modulus.

For simplicity and practical purposes, the actual nonlinear behavior, represented by Eq. (6), can be idealized by a bilinear elasto–plastic relationship as shown in Fig. 3 and expressed by Eq. (7).

$$P = k_{p1}\lambda \text{ for } \lambda < \lambda_0 \tag{7a}$$

$$P = P_0 + k_{p2}(\lambda - \lambda_0) \text{ for } \lambda_0 < \lambda < \lambda_u \tag{7b}$$

In the above equations, P_o and λ_o are the shear force and companion slip of the connector at the end of the elastic state while P_u and λ_u are the corresponding quantities at failure. The nonlinearity of the composite section can be captured by considering the nonlinearity of its constituent components via their moment–curvature relationships.

The moment–curvature (M–χ) diagrams for a reinforced concrete slab can be obtained for any section using the requirements of equilibrium and compatibility as explained in Appendix A. Using the procedure described in the foregoing appendix, for both the reinforced concrete and steel section, the latter relationship would be generally nonlinear as shown by the solid curve in Fig. 4. For practical purposes, the nonlinear $M_c - \chi$ response can be reasonably accurately approximated as a trilinear curve as shown in Fig. 4. In the figure, the moments M_{cr}, M_y and M_u, respectively, represent the reinforced concrete section cracking, yielding and ultimate moment, respectively, while χ_{cr}, χ_y and χ_u, denote the corresponding curvatures.

The slope of the three linear segments of the idealized moment–curvature curve are denoted by k_{c1}, k_{c2} and k_{c3}, which represent the flexural rigidity of the three commonly observed states of a reinforced concrete section, viz. uncracked, cracked-unyielded and cracked-yielded, henceforth designated as State 1, 2 and 3, respectively. With reference to Fig. 4, for the above states, one can write

$$M_c = k_{c1}\chi \text{ for } \chi < \chi_{cr} \tag{8a}$$

$$M_c = M_{cr} + k_{c2}(\chi - \chi_{cr}) \text{ for } \chi_{cr} < \chi < \chi_{cy} \tag{8b}$$

$$M_c = M_{cy} + k_{c3}(\chi - \chi_{cy}) \text{ for } \chi_{cy} < \chi < \chi_{cu} \tag{8c}$$

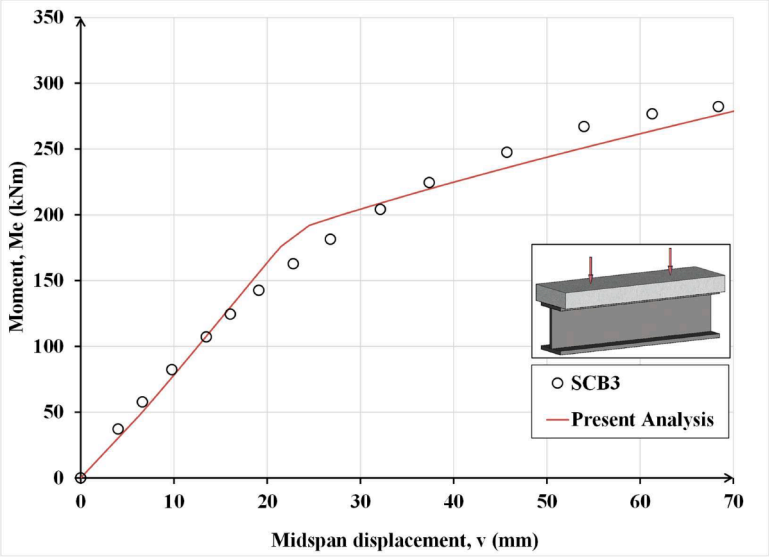

Fig. 13. Computed and experimental midspan moment–displacement curve for beam SCB3 in case (b).

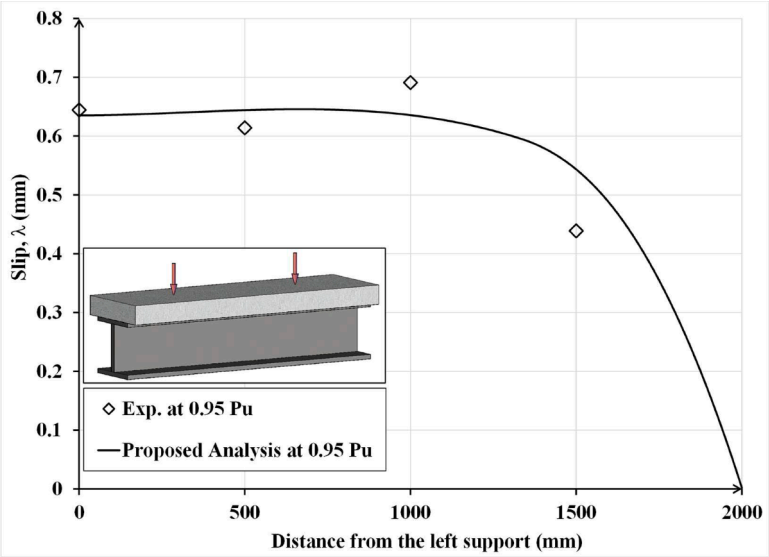

Fig. 14. Computed and experimental slip curves for beam SCB1 in case (b) at 95 % of the beam failure load, P_u.

For the steel section, assuming steel to behave as an elasto–plastic strain hardening material, its nonlinear moment–curvature relationship can be represented by a bilinear approximation as shown in Fig. 5. These approximations are in conformity with past studies and sufficiently accurate for practical applications, as will be demonstrated later in the present investigation. With reference to Fig. 5,

$$M_s = k_{s1}\chi \text{ for } \chi < \chi_{sy} \tag{9a}$$

$$M_s = k_{s2}(\chi - \chi_{su}) \text{ for } \chi_{sy} < \chi < \chi_{su} \tag{9b}$$

where k_{s1} and k_{s2} are the slopes of the two linear segments in the idealized moment–curvature relationship of the steel section (Fig. 5a). Similarly, m_{s1} and m_{s2} are the axial rigidity for State 1 and 2, respectively. By satisfying the compatibility (Eq. (1)) and equilibrium (Eq. (2) and (3)) requirements, and by using the interface shear–slip relationship (Eq. (4)) and the constitutive relations (Eq. (5)), the solution of the governing equations can be obtained, depending on the evolution of interfacial slip and the state of the steel–concrete composite section as explained below.

(i) *For Slip Level I:* $\lambda \leq \lambda_o$

Since slip is independent of the state of the cross-section, at any slip level, the steel–concrete composite section could be in any of the abovementioned states. The governing equation can be solved for each state, subject to the $\lambda \leq \lambda_o$ constraint as shown below.

Considering Eq. (1) and the shear–slip relationship in Fig. 3, the rotation of the steel–concrete composite section, ϕ, can be expressed as:

$$\phi = \left(u_s - u_c - \frac{s}{k_{p1}}\frac{dP}{dx}\right)\frac{1}{d} \tag{10}$$

(ii) *For Slip Level II:* $\lambda_o < \lambda \leq \lambda_u$

For slip level II, an equation, like Eq. (10), can be written as

$$\phi = \left[u_s - u_c - \frac{s}{k_{p2}}\left(\frac{dP}{dx} - \frac{P_0 - k_{p2}\lambda_0}{s}\right)\right]\frac{1}{d} \tag{11}$$

In view of Eqs. (10) and (11), the curvature, χ, is

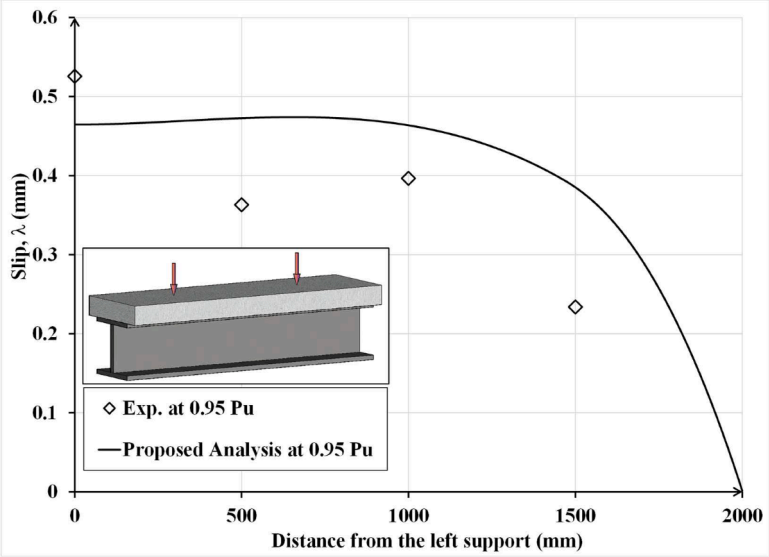

Fig. 15. Computed and experimental slip curves for beam SCB2 in case (b) at 95 % of the beam failure load, P_u.

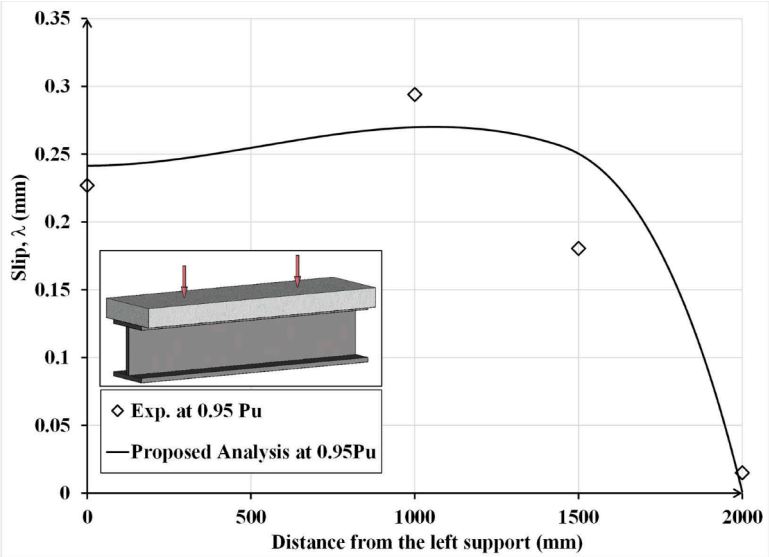

Fig. 16. Computed and experimental slip curves for beam SCB3 in case (b) at 95 % of the beam failure load, P_u.

$$\chi = \frac{d\phi}{dx} = \left(\varepsilon_s - \varepsilon_c - \frac{s}{k_{pk}}\frac{d^2P}{dx^2}\right)\frac{1}{d} \tag{12}$$

It is important to underline that the expression of curvature for either slip level (I or II), assumes the same form but the slip level will depend on the subscript k in Eq. (12), with $k = 1$ for $\lambda \leq \lambda_o$ and $k = 2$ for $\lambda_o < \lambda \leq \lambda_u$.

Substituting in Eqs. (10) or (11) Eqs. (2), (4), (8) and (9), it is possible to obtain the following second order differential equation

$$\frac{d^2P}{dx^2} - \omega_p^2 P + \frac{\omega_p^2}{b_p^2}(M_e + M^*) \tag{13}$$

where M_e is the external moment acting at section x while M^* and $\omega_p = a_p b_p$ are numerical parameters that are function of the external load.

It is important to underline that a second order differential equation having the same form as Eq. (13) must be written for each state, depending on the states of the concrete slab and the steel profile as described in more detail below.

The general solution of Eq. (13) can be written as

$$P(x) = Ae^{\omega_p x} + Be^{-\omega_p x} + \frac{(M_e + M^*)}{b_p^2} \tag{14}$$

Considering Eq. (14) and the moment–curvature relationships for the concrete slab in Fig. 4 and for the steel profile in Fig. 5, after some algebraic manipulations, the parameter ω_p and the moment M^*, can be derived, for any of level of loading as shown below. Furthermore, the integration constants A and B can be evaluated based on the boundary conditions of the beam. For a symmetrically loaded simply supported beam:

$$P(0) = 0 \tag{15a}$$

$$\frac{dP}{dx}\left(\frac{L}{2}\right) = 0 \tag{15b}$$

(i) Concrete slab uncraked and the steel profile in the elastic state

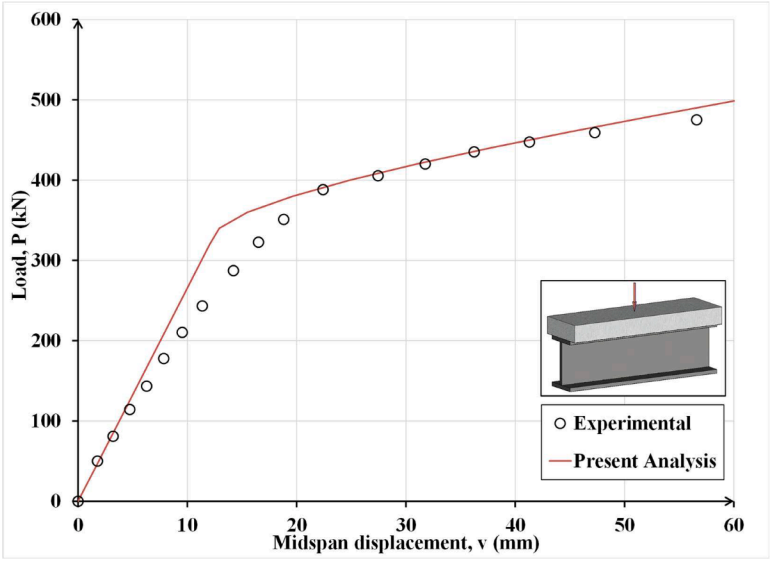

Fig. 17. Computed and experimental load–midspan displacement curve for beam in case (c).

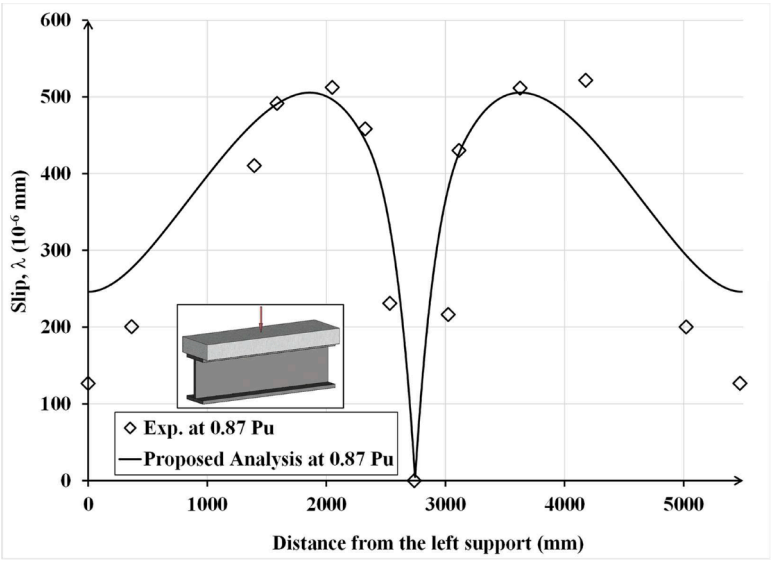

Fig. 18. Computed and experimental slip curves along the beam length at 87 % of the beam failure load for the beam in Case (c).

$$\omega_p = a_p(b_p) = \frac{k_{pk}d}{s(k_{c1}+k_{s1})}\left(\frac{k_{c1}+k_{s1}}{m_{ij}^{*}d}+d\right) \text{ and } M* = 0 \tag{16}$$

(ii) Concrete slab cracked and the steel profile in the elastic state

$$\omega_p = \frac{k_{pk}d}{s(k_{c2}+k_{s1})}\left(\frac{k_{c2}+k_{s1}}{m_{ij}^{*}d}+d\right) \text{ and } M^{*}$$
$$= k_{c2}\chi_{cr} - M_{cr} - \frac{s(k_{c2}+k_{s1})}{k_{pk}d}\left[\left(\frac{m_{c1}-m_{c2}}{m_{c2}}\right)\varepsilon_{cr}\right] \tag{17}$$

(iii) Concrete slab yielded and the steel profile in the elastic state

$$\omega_p = \frac{k_{pk}d}{s(k_{c3}+k_{s1})}\left(\frac{k_{c3}+k_{s1}}{m_{ij}^{*}d}+d\right) \text{ and}$$
$$M^{*} = k_{c3}\chi_{cy} - M_{cy} - \frac{s(k_{c3}+k_{s1})}{k_{pk}d}\left[\left(\frac{m_{c1}-m_{c2}}{m_{c3}}\right)\varepsilon_{cr} + \left(\frac{m_{c2}-m_{c3}}{m_{c3}}\right)\varepsilon_{cy}\right] \tag{18}$$

(iv) Concrete slab yielded and the steel profile yielded

$$\omega_p = \frac{k_{pk}d}{s(k_{c3}+k_{s2})}\left(\frac{k_{c3}+k_{s2}}{m_{ij}^{*}d}+d\right) \text{ and}$$
$$M^{*} = k_{c3}\chi_{cy} + k_{s2}\chi_{sy} - M_{cy} - M_{sy} + \ldots$$
$$\ldots - \frac{s(k_{c3}+k_{s2})}{k_{pk}d}\left[\left(\frac{m_{c1}-m_{c2}}{m_{c3}}\right)\varepsilon_{cr} + \left(\frac{m_{c2}-m_{c3}}{m_{c3}}\right)\varepsilon_{cy} - \left(\frac{m_{s1}-m_{s2}}{m_{s2}}\right)\varepsilon_{sy}\right] \tag{19}$$

where m_{ij}^{*} ($i = 1,2,3$ and $j = 1,2$) is

$$m_{ij}^{*} = \frac{m_{ci}m_{sj}}{m_{ci}+m_{sj}} \tag{20}$$

Note, m_{ci} ($i = 1,2,3$) is the axial rigidity of the concrete section at state i and m_{sj} ($j = 1,2$) is the axial rigidity of the steel profile at state j. The parameter b_p as noted from Eq. (16) to (28) is defined as $\left(\frac{k_{ci}+k_{sj}}{m_{ij}^{*}}+d\right)$ with $i = 1,2,3$ and $j = 1,2$.

Furthermore, after some manipulations of Eq. (2), the governing

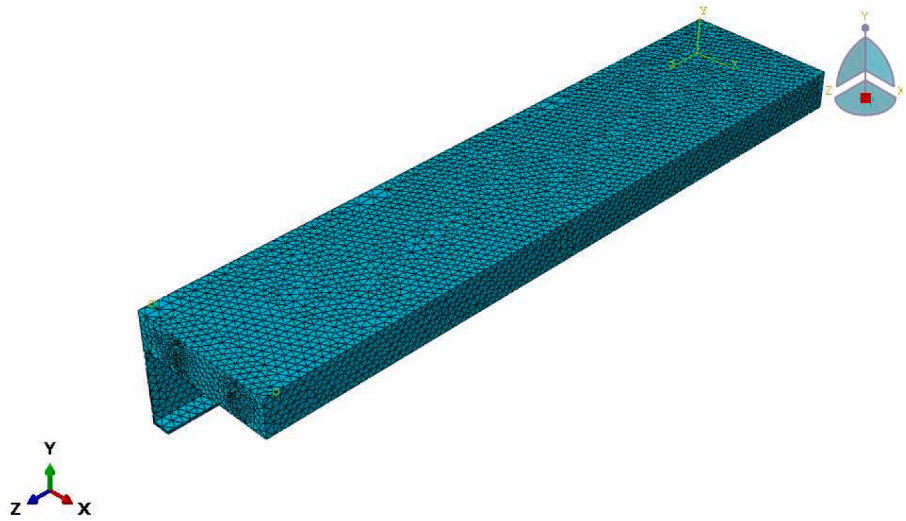

Fig. 19. Finite element mesh for the idealized quarter of the steel–concrete composite beam.

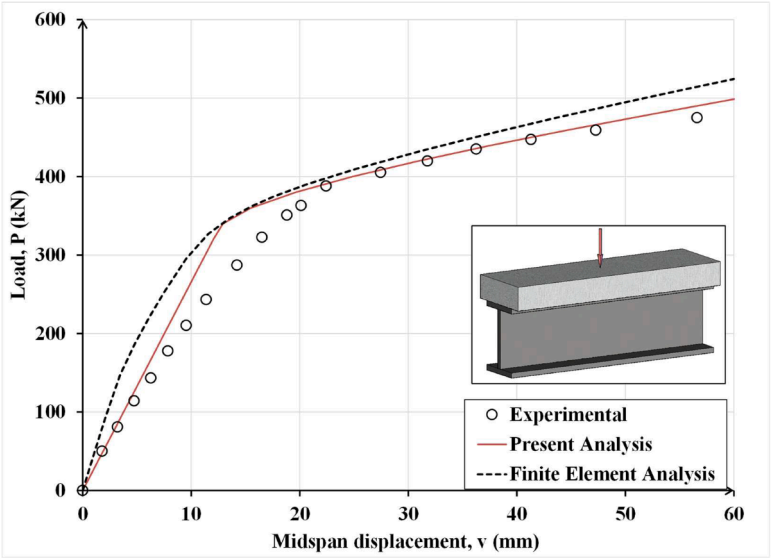

Fig. 20. Load–midspan deflection curve of the composite beam in case (c) given by finite element analysis and the proposed method.

equation of curvature can be obtained corresponding to State 1,2 and 3 of concrete slab and State 1 of steel profile respectively, as given by Eqs. (21a) –(21c), respectively

$$\chi(x) = \frac{M_e - Pd}{k_{c1} + k_{s1}} \tag{21a}$$

$$\chi(x) = \frac{M_e - Pd - M_{cr} + k_{c2}\chi_{cr}}{k_{c2} + k_{s1}} \tag{21b}$$

$$\chi(x) = \frac{M_e - Pd - M_{cy} + k_{c3}\chi_{cy}}{k_{c3} + k_{s1}} \tag{21c}$$

The solutions of curvature corresponding to State 2 and 3 of concrete slab and State 2 of steel profile, respectively, are given by Eqs. (22a) and (22b), respectively

$$\chi(x) = \frac{M_e - Pd - M_{cr} + k_{c2}\chi_{cr} - M_{sy} + k_{s2}\chi_{cy}}{k_{c2} + k_{s2}} \tag{22a}$$

$$\chi(x) = \frac{M_e - Pd - M_{cr} + k_{c2}\chi_{cr} - M_{sy} + k_{s2}\chi_{cy}}{k_{c3} + k_{s2}} \tag{22b}$$

The rotation $\phi(x)$ and the vertical displacement $v(x)$ at any section along the beam is computed by integration of the beam curvature as

$$\phi(x) = \int \chi(x)dx \tag{23}$$

$$v(x) = \int\int \chi(x)dx \tag{24}$$

3. Beam deflection calculation

As stated earlier, the beam rotation and deflection can be determined using Eqs. (23) and (24). However, the correct expression for the curvature must be selected. At points along the beam where there is abrupt change in the beam state, one must choose the appropriate curvature expressions for the segments to the right and the left of the transition point while concurrently satisfying the equality of displacement and rotation of the two segments at their common point. Therefore, inserting for curvature from Eqs. (21a) to (22b) into Eq. (24) leads to the following three equations for the deflected shape of the beam.

(i) Beam deflection equations for the concrete section being in States 1,2

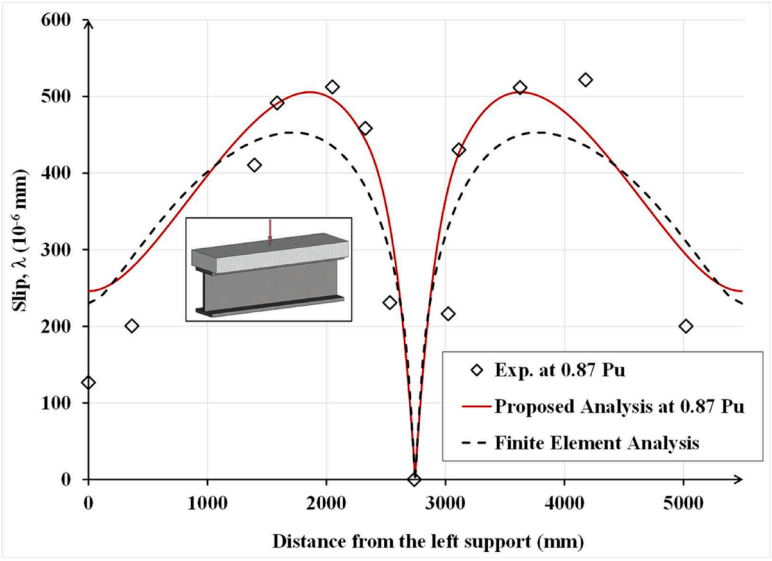

Fig. 21. Comparison of the FE and the proposed model predicted load–slip response of the composite beam with the associated experimental data.

or 3, respectively and the steel section being in State 1

$$v(x) = \frac{1}{(k_{c1} + k_{s1})}\left[\int\int (M_e + M^*)dx^2 - \frac{1}{\omega_p^2}(Ae^{\omega_p x} + Be^{-\omega_p x})\right] + Cx + D \tag{25a}$$

$$v(x) = \frac{1}{(k_{c2} + k_{s1})}\left[\int\int (M_e + M^*)dx^2 - \frac{1}{\omega_p^2}(Ae^{\omega_p x} + Be^{-\omega_p x}) - \frac{1}{2}(M_{cr} - k_{c2}\chi_{cr})x^2\right] + Cx + D \tag{25b}$$

$$v(x) = \frac{1}{(k_{c3} + k_{s1})}\left[\int\int (M_e + M^*)dx^2 - \frac{1}{\omega_p^2}(Ae^{\omega_p x} + Be^{-\omega_p x}) - \frac{1}{2}(M_{cy} - k_{c3}\chi_{cy})x^2\right] + Cx + D \tag{25c}$$

(ii) Beam deflection equations for the concrete section being in State 2 or 3, respectively, and the steel section being in State 2

$$v(x) = \frac{1}{(k_{c2} + k_{s2})}\left[\int\int (M_e + M^*)dx^2 - \frac{1}{\omega_p^2}(Ae^{\omega_p x} + Be^{-\omega_p x}) + \ldots \right.$$
$$\left. \ldots - \frac{1}{2}(M_{cr} - k_{c2}\chi_{cr} + M_{sy} - k_{s2}\chi_{sy})x^2\right] + Cx + D \tag{26a}$$

$$v(x) = \frac{1}{(k_{c3} + k_{s2})}\left[\int\int (M_e + M^*)dx^2 - \frac{1}{\omega_p^2}(Ae^{\omega_p x} + Be^{-\omega_p x}) + \ldots \right.$$
$$\left. \ldots - \frac{1}{2}(M_{cy} - k_{c3}\chi_{cy} + M_{sy} - k_{s2}\chi_{sy})x^2\right] + Cx + D \tag{26b}$$

The constants $C_{i,j}$ and $D_{i,j}$ (i = *I,II;* j = *1,2,3*) are determined by applying the following boundary conditions:

$$v\left(\frac{L}{2}\right) = 0 \tag{27a}$$

$$v'(0) = 0 \tag{27b}$$

Additional constraints are imposed on the solution to ensure equality of displacement and rotation of the beam at the common point of adjacent segments. These constraints, together with the above boundary conditions, provide sufficient equations to solve for the unknown constants of integration.

3.1. Numerical solution scheme

The beam is divided into several finite segments and since the problem is nonlinear, the load is applied incrementally. Initially, all the segments will be uncracked (State 1) and will have zero slip (slip level I), thus the solution would be based on linear elasticity. Therefore, depending on its slip level and the stress state, the appropriate flexural rigidity, curvature and deflection equation need to be applied. At the common point of two adjacent segments x_i and x_{i+1}, the following continuity conditions must be satisfied:

$$P_{i,j}(x_i) = P_{i,j}(x_{i+1})\,(\text{continuity of shear force}) \tag{28a}$$

$$\frac{dP_{i,j}(x_i)}{dx} = \frac{dP_{i,j}(x_{i+1})}{dx}\,(\text{continuity of interfacial shear flow}) \tag{28b}$$

and

$$v_{i,j}(x_i) = v_{i,j}(x_{i+1})\,(\text{continuity of vertical displacement}) \tag{29a}$$

$$\frac{dv_{i,j}(x_i)}{dx} = \frac{dv_{i,j}(x_{i+1})}{dx}\,(\text{continuity of rotation}) \tag{29b}$$

Due to the nonlinear nature of the problem, the solution must be incrementally and iteratively performed, and the iteration at the end of each increment can be terminated once a pre-selected convergence criterion is satisfied. At the common point of adjoining segments, the convergence criterion is calculated after each iteration and if the

difference between two consecutive iterations is less than or equal to a convergence tolerance ρ, the iteration process is terminated. In the present analysis, at the transition points of the beam from one stress state to another, it is checked to make sure the moment corresponds to either M_{cr} (at transition from State 1 to 2) or M_{cy} (at transition from State 2 to 3) for concrete slab and M_{sy} (at transition from State 1 to 2) for the steel profile. Finally, at the common point of each of the adjoining segments, the slip exhibited at the interface between the concrete slab and steel profile is monitored to determine whether $\lambda < \lambda_0$ or $\lambda > \lambda_0$, and the appropriate stiffness of the shear connectors is used.

The flowchart in Fig. 6 further details the nonlinear analysis procedure.

4. Validation of the theoretical model

To assess the robustness and accuracy of the proposed model, some steel–concrete composite beams, previously tested to failure by others, are analyzed. All the beams were simply supported and tested in four-point bending. The relevant properties of the beams are presented in Table 1. As the values of certain parameters in the tests were not reported, reasonable values are assumed for them in the current calculations, and the assumed values are indicated in italics in Table 1. These values are chosen based on known values in the literature for similar parameters.

The beams were tested in the laboratory by Xing et al. [48], Zhao et al. [49] and Chapman et al. [50].

In Table 1, the beams in the above studies are categorized as Case (a), (b) and (c), respectively. As may be observed in the table, in some of these investigations, more than one beam was tested.

Fig. 7 shows for the duplicate beams FBST-1 and FBST-2, tested in Case (a), the computed and experimentally measured load–midspan deflection curves.

Fig. 8 shows for the last two beams the computed and experimentally measured load–slip variation under increasing load until failure.

It is important to underline that the above results are obtained by assuming a bilinear shear force-slip relationship for the shear connectors.

Fig. 9 shows for the beam FBST-3 in Case (a), the computed and experimentally measured load–midspan deflection up to failure.

Fig. 10 shows for the duplicate beams FBST-4 and FBST-5 in Case (a), the computed and experimentally measured load–midspan deflection up to failure.

Figs. 11–13 show the computed and corresponding experimentally measured midspan moment-displacement curves for the beams tested in Case (b). Notice, with reference to Table 1, in Case (b), beams with the same dimensions but different concrete or steel strength were tested, which are designated as SCB1, SCB2 and SCB3.

Figs. 14–16 show the computed and corresponding experimentally measured slip along the concrete slab-steel girder interface at 95 % of the failure load, P_u, for beams SCB1, SCB2 and SCB3, respectively.

Fig. 17 shows the computed and experimental load–midspan deflection curves of the beam tested by Chapman and Yam [50], whose details are given in Table 1 under Case (c), while Fig. 18 illustrates the same beam load–slip curve at 87 % of its failure load.

The above comparisons demonstrate that the proposed method of analysis can relatively accurately predict the complete response of the tested beams up to failure, including the slip at the concrete slab-steel girder interface, which affects the degree of interaction between the two elements of the composite beam. Although differences exist in the preceding figures between the experimental and corresponding computed deflections and slip values, some of these differences can be ascribed to the random variations of material properties in the tested beams. The sensitivity of the measuring devices and the inevitable variation in the execution of the test. This is evident from the load–deflection curves of nominally identical beams BFTF-1 and BFTF-2 in Fig. 7 or the duplicate beams BFTF-5 and BFTF-6 in Fig. 10. Similarly, for the symmetrical beam tested in Case (c), the experimentally measured slip values for the two halves of the beam are not identical. It should be pointed out that accurate measurement of interface slip in physical tests is a difficult task, especially at the later stages of loading. Despite these differences, the writers believe that the results of the current analyses are sufficiently accurate for practical design and analysis.

5. Comparison between the results of the proposed analysis method and the general finite element analysis

In this section the accuracy of the proposed method is compared with that of the FE analysis by a commercial software package [51]. The beam that is analyzed for this comparison is the one referred to as Case (c) in Table 1. Due to double symmetry of the beam, in the FE analysis, only a quarter of it is discretized. A total of 526,653 three-dimensional 10-node quadratic tetrahedron (C3D10) elements with maximum side length of 30 mm are used as illustrated in Fig. 19. Contact elements are used to model the behavior of the shear connectors.

The load–midspan deflection of the analyzed beam, obtained by finite element, is compared in Fig. 20 with that given by the proposed semi-analytic procedure.

The last figure shows that the two curves are reasonably close but, as expected, the proposed analysis results appear to be more accurate, albeit from the practical perspective, the differences are not significant. As load–deflection prediction is not always the best indicator of the robustness and accuracy of a model, in Fig. 21, the load–slip curves predicted by the two models are compared with the corresponding experimental data for the same beam. Both models reasonably accurately predict the slip variation, but again the proposed model seems to give somewhat better results.

Consequently, given the minimal time required to perform the analysis by the proposed method and the relative accuracy of the method, it can be a useful and expedient method for analyzing the behavior of statically determinate steel–concrete partially or fully composite beams over the full loading range until failure. It can be used to gauge the effect of the extent of composite action conveniently and rapidly on the serviceability and strength of steel–concrete composite beams.

6. Conclusions

In this paper a novel and relatively simple analytical model is proposed to predict the full response of partially interacting steel–concrete composite beams. This model can be applied to beams and one-way slabs subjected to any concentrated or uniform load or their combinations. Its robustness and accuracy are verified by comparing its results with the corresponding experimental data for several beams in the literature. Accordingly, the following principal conclusions are reached regarding the proposed model:

1) The model can consider steel and concrete nonlinearity, the advent of cracking and tension-stiffening in concrete as well steel yielding and strain hardening on steel–concrete composite beams ultimate strength and flexural response.
2) It can explicitly consider the presence and effect of steel reinforcement in the concrete slab on the composite beam flexural response and ultimate strength.
3) It can provide the nonlinear interfacial shear stress and associated slip distribution along the steel girder and concrete slab interface at any load level up to failure.
4) It can accurately and rapidly, with minimal input data, predict the ultimate load capacity and complete flexural response of partially interacting steel–concrete composite beams, and its results compare well with those given by the more general and time-consuming nonlinear finite element analysis.

CRediT authorship contribution statement

Marco Lamberti: Writing – review & editing, Writing – original draft, Visualization, Validation, Software, Methodology, Investigation, Formal analysis, Data curation, Conceptualization. **Ghani Razaqpur:** Writing – review & editing, Visualization, Validation, Resources, Methodology, Funding acquisition, Conceptualization, Project administration.

Declaration of competing interest

The authors declare that they have no known competing financial interests or personal relationships that could have appeared to influence the work reported in this paper.

Data availability

Data will be made available on request.

Acknowledgments

The authors are grateful to the State Administration of Foreign Experts of China, the Tianjin Municipal Government and Nankai University for their financial support of this research collaboration through grants [C021801601] and [BE044741] awarded to Professor Razaqpur.

Appendix A

In this appendix the nonlinear constitutive laws of concrete and steel are used in conjunction with strain compatibility and equilibrium requirements to derive the nonlinear moment curvature and force-strain relationship of the reinforced concrete slab and the steel girder. For the slab, the adopted constitutive laws for concrete in compression and tension and for steel rebars are shown in Fig. A1. The concrete in compression is modeled by the Thornenfeld et al. [52] proposed stress-strain relationship, represented by Eq. (A1), which is suitable for concrete strengths up to 100 MPa.

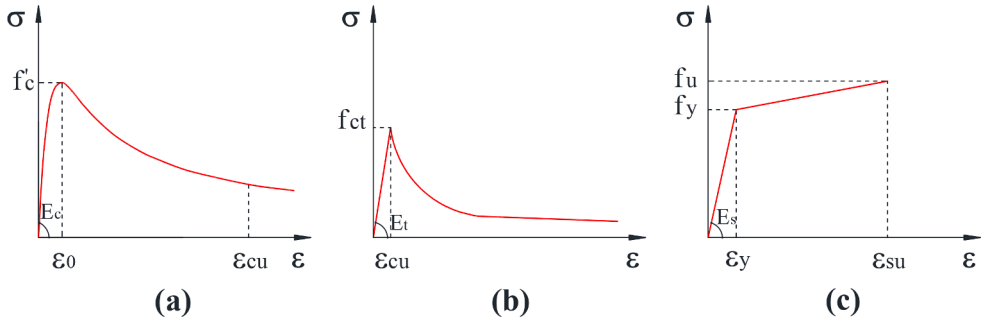

Fig. A1. Stress–strain relationship: a) concrete in compression, b) concrete in tension; c) steel bars.

$$\frac{\sigma_c}{f'_c} = \frac{n\left(\frac{\varepsilon_c}{\varepsilon_0}\right)}{n - 1 + \left(\frac{\varepsilon_c}{\varepsilon_0}\right)^{nk}} \tag{A1}$$

where $\sigma_c$and ε_c are the concrete compressive stress and strain, respectively, $f'_c$is the peak stress obtained from a cylinder test, $\varepsilon_0$the strain corresponding to f'_c, n is a curve-fitting factor equal to $\frac{E_c}{(E_c - E'_c)}$, E_c is the initial tangent modulus, E'_c is equal to $\frac{f'_c}{\varepsilon_0}$ and k is a factor to control the slopes of the ascending and descending branches of the stress-strain curve, with $k = 1.0$ for $\frac{\varepsilon_c}{\varepsilon_0} \leq 1.0$ and $k > 1.0$ for $\frac{\varepsilon_c}{\varepsilon_0} > 1.0$. For the choice of the appropriate n and k values for a specific concrete, reference should be made to [52].

The concrete in tension is modeled as linear elastic before cracking and as a strain-softening material after cracking as illustrated in Fig. A1(b) and expressed by Eqs. (A2(a)) and (b), respectively.

$$\sigma_{ct} = E_t \varepsilon_{ct} \text{ for } \varepsilon_c \leq \varepsilon_{to} \text{ with } E_t = \frac{E_c}{2}, \varepsilon_{to} = \frac{f_t}{E_t} \tag{A2a}$$

$$\sigma_{ct} = f_t \left(\frac{\varepsilon_{ct}}{|\varepsilon_{to}|}\right)^c \text{ for } \varepsilon_{ct} > \varepsilon_{to} \tag{A2b}$$

where E_t is the elastic modulus of concrete in tension, f_t is the absolute value of its tensile strength and ε_{to} is its corresponding strain. The power c in Eq. (A2b) controls the shape of the softening branch of curve. Its value will depend on the RC section geometric and mechanical properties. Typically, it ranges between 0.2 and 0.6 [53], but further discussion is beyond the scope of this study.

For the steel reinforcement or girder, a typical bilinear stress-strain relationship is adopted as in Fig. A2(c), which is expressed as

$$\sigma_s = E_s \varepsilon_s \text{ for } \varepsilon_s \leq \varepsilon_y \text{ with, } \varepsilon_y = \frac{f_y}{E_s} \tag{A3a}$$

$$\sigma_s = \frac{f_u - f_y}{\varepsilon_{su} - \varepsilon_y} \varepsilon_s \text{ for } \varepsilon_y < \varepsilon_s < \varepsilon_{su} \tag{A3b}$$

where E_s, f_y, ε_y, f_u and ε_{su} are the elastic modulus, yield stress, yield strain, ultimate strength and ultimate strain of the reinforcing steel.

The following flowchart shows how the requirements of strain compatibility and equilibrium can be used in conjunction with the above constitutive laws to obtain the moment–curvature and axial force-extreme fiber strain relationship for a typical reinforced concrete or steel section. It should be emphasized that these properties are determined for the concrete slab and the steel girder separately and they do not involve any composite action between the two parts.

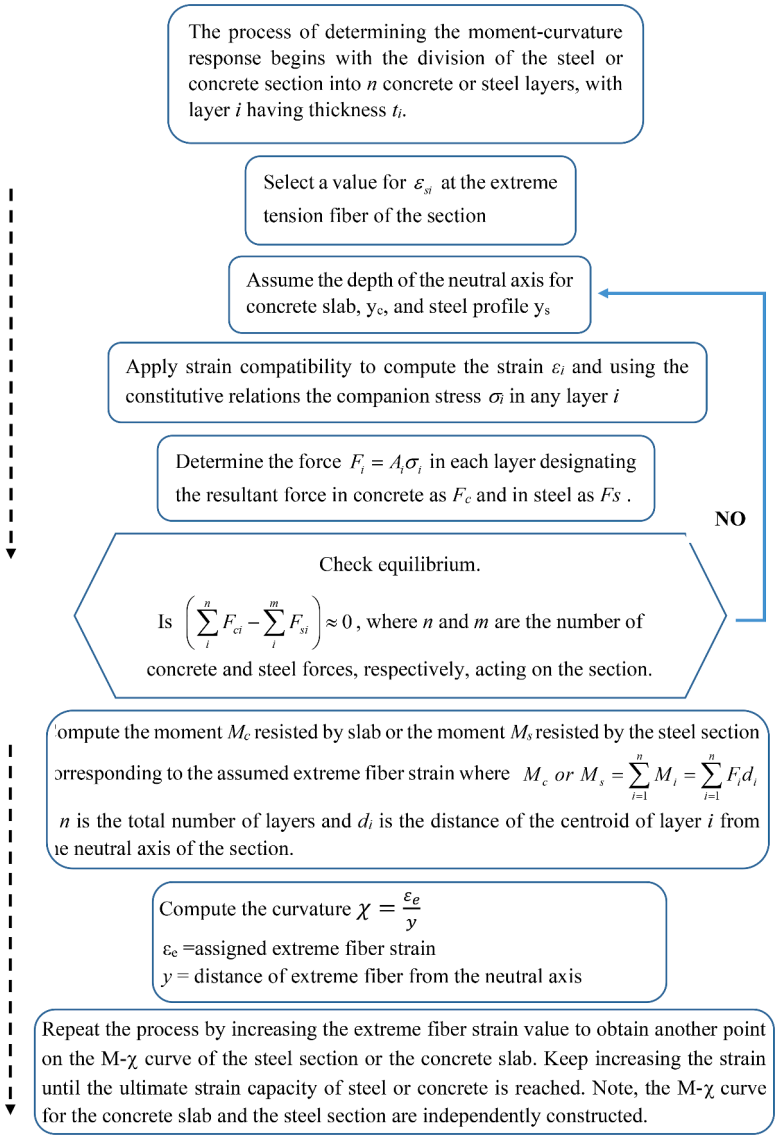

Fig. A2. Flowchart for computing the typical moment–curvature relationships for the reinforced concrete one-way slab or steel section.

References

[1] Fabbrocino G., Pecce M. Experimental on steel-concrete composite beams under negative bending. Conference: 2000 Annual Conference Abstracts - Canadian Society for Civil Engineering.

[2] Y.-H. Wang, J. Yu, J.-P. Liu, F Chen, Experimental study on assembled monolithic steel-concrete composite beam in positive moment, Eng. Struct. 180 (2019) 495–509.

[3] E. Ellobody, B. Young, Performance of shear connection in composite beams with profiled steel sheeting, J. Constr. Steel Res. 62 (2006) 682–694.

[4] N.M. Newmark, C.P. Siess, I.M Viest, Tests and analysis of composite beams with incomplete interaction, Proc. Soc. Exp. Stress Anal. 9 (1) (1951) 75–92.

[5] J. Eom, A.S Nowak, Live load distribution for steel girder bridges, J. Bridge Eng. 6 (2001) 489–497.

[6] K. Phuvoravan, W. Chung, J. Liu, E.D Sotelino, Simplified live load distribution factor equation for steel girder bridges, J. Trans. Res. Board 1892 (2004) 88–97.

[7] Z. Yousif, R. Hindi, AASHTO_LRFD live load distribution for beam-and-slab bridges: limitations and applicability, J. Bridge Eng. 12 (2007) 765–773.

[8] E. Spacone, S. El-Tawil, Nonlinear analysis of steel concrete composite structures: state of the art, J. Struct. Eng. 130 (2004) 159–168.

[9] P. Foraboschi, Analytical solution of two-layer beam taking into account nonlinear interlayer slip, J. Eng. Mech. 135 (2009) 1129–1146.

[10] Y.F. Wu, D.J. Oehlers, M.C Griffith, Partial-interaction analysis of composite beam/column members, Mech. Struct. Mach. 30 (2007) 309–332.

[11] U.A. Girhammar, V.K Gopu, Composite beam-columns with interlayer slip exact analysis, J. Struct. Eng. 119 (1993) 1265–1282.

[12] U.A. Girhammar, D.H Pan, Exact static analysis of partially composite beams and beam-columns, Int. J. Mech. Sci. 49 (2007) 239–255.

[13] J.-P. Lin, G. Wang, G. Bao, R. Xu, Stiffness matrix for the analysis and design of partial-interaction composite beams, Constr. Build. Mater. 156 (2017) 761–772.

[14] R. Xu, D. Chen, Variational principles of partial-interaction composite beams, J. Eng. Mech. 138 (2011) 542–551.

[15] R. Xu, Y. Wu, Static, dynamic, and buckling analysis of partial interaction composite members using Timoshenko's beam theory, Int. J. Mech. Sci. 49 (2007) 1139–1155.

[16] R. Xu, G. Wang, Variational principle of partial-interaction composite beams using Timoshenko's beam theory, Int. J. Mech. Sci. 60 (2012) 72–83.

[17] S. Schnabl, M. Saje, G. Turk, I. Planinc, Analytical solution of two-layer beam taking into account interlayer slip and shear deformation, J. Struct. Eng. 133 (2007) 886–894.

[18] R. Xu, G. Wang, Bending solutions of the Timoshenko partial-interaction composite beams using Euler-Bernoulli solutions, J. Eng. Mech. 139 (2013) 1881–1885.
[19] Y. Wu, M.C. Griffith, D.J Oehlers, Numerical simulation of steel plated RC columns, Comput. Struct. 82 (2004) 359–371.
[20] Q. Nguyen, M. Hjiaj, S. Guezouli, Exact finite element model for shear deformable two-layer beams with discrete shear connection, Finite Elem. Anal. Des. 47 (2011) 718–727.
[21] M.R. Salari, E. Spacone, Finite element formulations of one-dimensional elements with bond-slip, Eng. Struct. 23 (2001) 815–826.
[22] Z. Shen, H. Zhong, Static and vibrational analysis of partially composite beams using the weak-form quadrature element method, Math. Probl. Eng. 7 (2012) 1–23.
[23] A. Ayoub, F.C Filippou, Mixed formulation of nonlinear steel-concrete composite beam element, J. Struct. Eng. 126 (2000) 371–381.
[24] C. Faella, E. Martinelli, E. Nigro, Steel and concrete composite beams with flexible shear connection: "exact" analytical expression of the stiffness matrix and applications, Comput. Struct. 80 (2002) 1001–1009.
[25] B. Čas, M. Saje, I. Planinc, Non-linear finite element analysis of composite planar frames with an interlayer slip, Comput. Struct. 82 (2004) 1901–1912.
[26] G. Ranzi, M.A. Bradford, B. Uy, A direct stiffness analysis of a composite beam with partial interaction, Int. J. Numer. Meth. Eng. 61 (2004) 657–672.
[27] G. Ranzi, M.A Bradford, Direct stiffness analysis of a composite beam-column element with partial interaction, Comput. Struct. 85 (2007) 1206–1214.
[28] G. Ranzi, A. Zona, A steel–concrete composite beam model with partial interaction including the shear deformability of the steel component, Eng. Struct. 29 (2007) 3026–3041.
[29] S.F. Jiang, X. Zeng, D. Zhou, Novel two-node linear composite beam element with both interface slip and shear deformation into consideration: formulation and validation, Int. J. Mech. Sci. 85 (2014) 110–119.
[30] Q. Nguyen, E. Martinelli, M. Hjiaj, Derivation of the exact stiffness matrix for a two-layer Timoshenko beam element with partial interaction, Eng. Struct. 2 (2011) 298–307.
[31] E. Martinelli, C. Faella, G.D. Palma, Shear-flexible steel-concrete composite beams in partial interaction: closed-form "exact" expression of the stiffness matrix, J. Eng. Mech. 138 (2012) 151–163.
[32] G. Razaqpur, M. Shedid, M. Nofal, Inelastic load distribution in multi-girder composite bridges, Eng. Struct. 44 (2012) 234–247.
[33] G. Razaqpur, M. Nofal, M. Shedid, A. Esfandiarid, Nonlinear behaviour of steel–concrete composite bridges: finite element modelling and experimental verification, Can. J. Civil Eng. 39 (2) (2012) 191–202.
[34] G. Razaqpur, M. Nofal, Analytical modeling of nonlinear behavior of composite bridges, J. Struct. Eng. 116 (6) (1990) 1715–1733.
[35] R. Brighenti, S. Bottoli, A novel finite element formulation for beams with composite cross-section, Int. J. Mech. Sci. 89 (2014) 112–122.
[36] J.P. Lin, J.F. Wang, R.Q Xu, Cohesive zone model based numerical analysis of steel-concrete composite structure push-out tests, Math. Probl. Eng. (2014) 1–12.
[37] J.B.M. Sousa, Da Silva A R, Nonlinear analysis of partially connected composite beams using interface elements, Finite Elem. Anal. Des. 43 (2007) 954–964.
[38] A.R. Da Silva, J.B.M Sousa, A family of interface elements for the analysis of composite beams with interlayer slip, Finite Elem. Anal. Des. 45 (2009) 305–314.
[39] J. Turmo, J.A. Lozano-Galant, E. Mirambell, D. Xu, Modeling composite beams with partial interaction, J. Constr. Steel. Res. 114 (2015) 380–393.
[40] U.K. Zhong Tao, K.M Hassan, Finite element modelling of steel-concrete composite beams with profiled steel sheeting, J. Constr. Steel. Res. 146 (2018) 1–15.
[41] M. Lasheen, A. Shaat, A. Khalil, Numerical evaluation for the effective slab width of steel-concrete composite beams, J. Constr. Steel Res. 148 (2018) 124–137.
[42] R. Shamass, K.A. Cashell, Analysis of stainless steel-concrete composite beams, J. Constr. Steel. Res. 152 (2019) 132–142.
[43] A. Amendola, J. de Castro Motta, G. Saccomandi, L. Vergori, Aconstitutive model for transversely isotropic dispersive materials, Proc. R. Soc. A480 (2024) 20230374.
[44] F. Fraternali, J. de Castro Motta, J. Germano, E. Babilio, A Amendola, Mechanical response of tensegrity-origami solar modules, Appl. Eng. Sci. 17 (2024) 100174.
[45] J. de Castro Motta, V. Zampoli, S. Chirita, M. Ciarletta, On the structural stability for a model of mixture of poroussolids, Math. Meth. Appl. Sci. 47 (2024) 4513–4529.
[46] F. Fraternali, J de Castro Motta, Mechanics of superelastic tensegrity braces for timber frames equipped with buckling-restrained devices, Int. J. Solids Struct. 281 (2023) 112414.
[47] J.D. Ollergaard, R.G. Slutter, J.W Fisher, Shear strength of stud connectors in light weight and normal-weight concrete, AISC Eng. J. 8 (1971) 55–64.
[48] Y. Xing, Q. Han, J. Xu, Q. Guo, Y. Wang, Experimental and numerical study on static behavior of elastic concrete-steel composite beams, J. Constr. Steel Res. 123 (2016) 79–92.
[49] H. Zhao, Y. Yong, Experimental studies on composite beams with high-strength steel and concrete, Steel Compos. Struct. 10 (2010) 297–307.
[50] J.C. Chapman, L.C.P Yam, The Inelastic behaviour of simply supported composite beams of steel and concrete, Proc. Inst. Civil Eng. 41 (1968) 651–683.
[51] S. Michael, ABAQUS/Standard Use's Manual, Version 6.9, Dassault Systèmes Simulia Corp, Providence, RI, USA, 2009.
[52] J.K. Wight, J.G. MacGregor, Reinforced Concrete: Mechanics and Design, Prentice Hall, N J, 2009.
[53] H. Okamura, K. Maekawa, S. Sivasubramaniyam, Verification of modeling for reinforced concrete finite element. Finite element analysis of reinforced concrete structures, ASCE (1985) 528–543.